This is a peer-reviewed, accepted author manuscript of the following research article: Hashem, A., Mohamed, L. A., Fletcher, A. J., Sanousy, M. A., Younis, H., & Mauof, H. (2021). Carboxylated cellulose for adsorption of Hg(II) ions from contaminated water: isotherms and kinetics. Journal of Polymers and the Environment. https://doi.org/10.1007/s10924-021-02075-9

Carboxylated cellulose for adsorption of Hg(II) ions from contaminated water: isotherms, kinetics, and thermodynamic studies

Abstract

Microcrystalline cellulose (MCC) was modified with 1, 2, 3, 4-butanetetracarboxylic acid (BTCA) to obtain the adsorbent material named treated microcrystalline cellulose (TMCC), which was characterized for point of zero charge (pHZPC), estimation of carboxyl group content and surface group moieties, surface morphology and textural properties. Application of TMCC for the removal of Hg(II) ions from aqueous solution was studied with respect to carboxyl group content, and process parameters, including adsorbent dose, initial solution pH, temperature, contact time, and Hg(II) ion concentration, to provide information about the adsorption mechanism. Isothermal adsorption data were analysed using a range of two and three parameter adsorption models, with the level of fit determined using nonlinear regression analysis. The maximum adsorption capacity under optimised conditions was determined using Langmuir analysis and found to be 1140 mg/g, and Freundlich analysis showed that adsorption of Hg(II) ions onto TMCC is favourable. The process was shown to be non-spontaneous and exothermic, via thermodynamic analysis while kinetic fits, using a range of models, showed that a pseudo-second order kinetic model was most appropriate for the data obtained, which indicates that the process involves chemisorption. The results obtained show TMCC to have a high affinity for Hg(II) ions from aqueous media, which suggests that these materials may have potential for application in water treatment systems.

Keywords: Microcrystalline cellulose; Isotherm models; kinetic models; FTIR; BET; SEM.

1. Introduction

Water contamination, due to elevated levels of large quantities of toxins or substances, such as harmful heavy metal ions, inorganic anions, micropollutants, organic compounds such as dyes, phenols, pesticides, humic substances, detergents, and other persistent organic pollutants, has been widely documented in various parts of the world in recent decades. The introduction of these toxic chemicals into the natural water sources has significant impact on the ecological balance, and adverse effects on flora and fauna. Some contaminants are not only resistant to chemical or biological degradation but also have high environmental resilience and a strong bioaccumulation potential in the food chain [1]. It is, therefore, important to treat polluted water and wastewater prior to its discharge into the natural environment to remove such species. Multiple treatment methods are required to minimise the concentrations of contaminants in water and wastewater, including chemical oxidation and reduction, membrane isolation, liquid extraction, ion exchange, electrolytic treatment, electron precipitation, coagulation, and flocculation [2-8]. Due to its high removal efficiency, without the production of harmful by-products, adsorption with activated carbon is considered one of the best alternative treatments for water and wastewater treatment [1]. In recent years, research has focussed on developing low cost, environmentally friendly materials for water and wastewater treatment, with no hazardous process by-products, resulting in increased attention towards natural bio-based materials, which also offer high uptake capacities, reduced sludge generation, regenerative potential, and abundant availability globally [9]. One such material is microcrystalline cellulose, which is also biodegradable, has good mechanical strength, and high thermal stability [10]. The adsorption capacity of this raw material has been enhanced by chemical modification of the cellulose backbone through chemical modification [11] . where chemical reactions (e.g. esterification, etherification, amination), graft copolymerization, or physicochemical modification (e.g. thermal or mechanical reinforcements) [12] can be utilised.

Within the gamut of water pollutants, heavy metals have been shown to be persistent and have significant adverse effects; of these mercury is known to be highly toxic, and the World Health Organization has set a limit of 6 µg/L of mercury in drinking water [13,14]. Exposure to raised levels may result in renal or pulmonary disorders [15], while consumption of methyl mercury via contaminated seafood by pregnant women can result in damage to the foetal nervous system [16]. Consequently, there has been significant effort to find efficient methods of Hg(II) ions from aqueous solutions [17], and this study focusses on the feasibility of using chemically treated microcrystalline cellulose such applications. Kinetic and thermodynamic data obtained for these systems was modelled to determine the physical parameters of the adsorption steps occurring and to inform about the mechanism of the process.

2. Materials and Methods

2.1. Materials

Microcrystalline cellulose (MCC), ~50 µm particle size, 1, 2, 3, 4-butanetetracarboxylic acid (BTCA), lead acetate, ethylenediaminetetraacetic acid (EDTA), nitric acid (HNO_3), sodium hydroxide (NaOH) and ethanol were supplied from Merck (Germany) and used as received (laboratory grade).

2.2. Methods

2.2.1. Preparation of the adsorbent

The treated microcrystalline cellulose (TMCC) was obtained by adding a known weight of butanetetracarboxylic acid (BTCA, dissolved in the least amount of water) to a 400 ml beaker containing 2 g of microcrystalline cellulose (MCC), the resulting mixture was stirred with a spatula until a homogeneous paste was obtained. The paste was subsequently transferred to a Petri dish and placed in an electric oven at 140°C for 2 h, before cooling to room temperature. Any soluble by-products and un-reacted BTCA was removed by washing the samples several times with a water:ethanol (20:80) mixture before drying at 70°C for 4 h. Three levels of modification of TMCC, to produce various degrees of carboxylation, were achieved by keeping all other reaction conditions constant, while varying the amount of butanetetracarboxylic acid. The degree of carboxylation obtained is shown in Table 1. It is evident that the extent of esterification increases significantly by increasing BTCA concentration within the range studied. This is likely due to the greater availability of BTCA molecules, which are converted to the anhydride form at high temperatures, as employed here, and subsequently react with the hydroxyl groups of MCC to form TMCC. It is likely that the high temperatures and longer reaction times used in this study would promote crosslinking within the structure (Scheme 1).

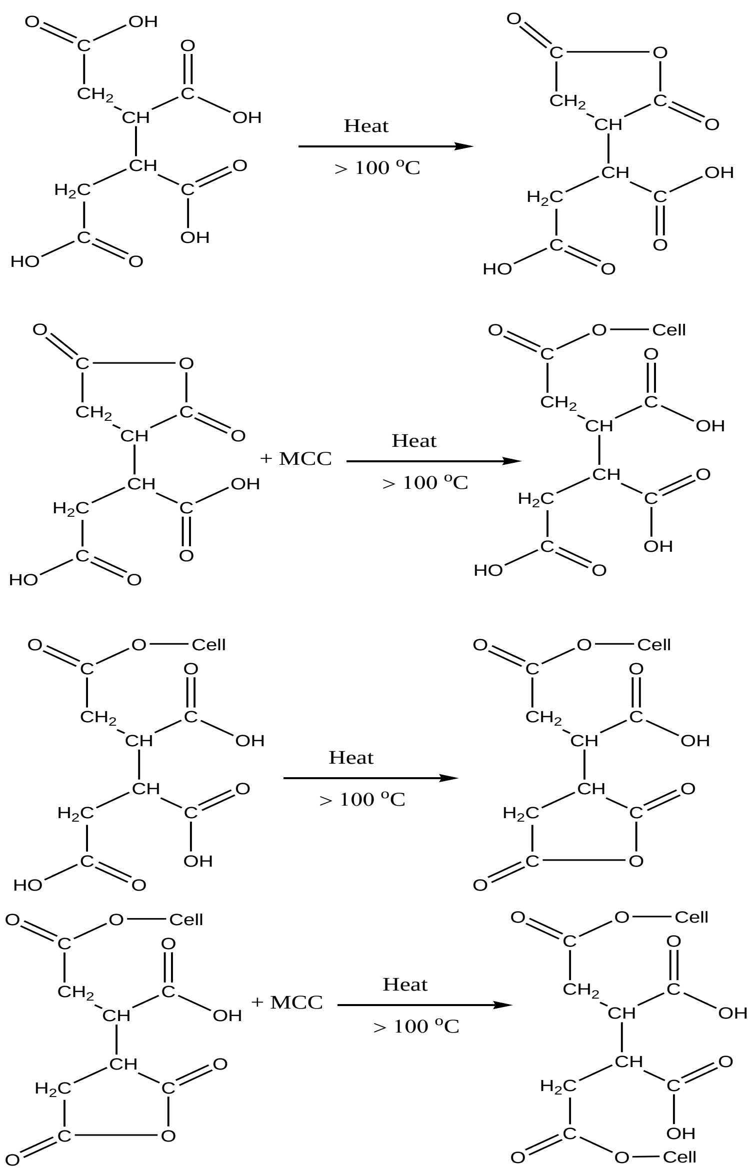

Scheme 1: Reaction between MCC and BTCA at 140 °C.

2.2.2. Batch Adsorption Studies

0.03 g of adsorbent was added to 100 mL of a Hg(II) ion solution (100–1000 mg/L) in a 125 mL Erlenmeyer flask, and 0.1 M HNO_3 or 0.1 M NaOH was added dropwise to regulate initial pH values. The mixture was shaken at 30°C and a continual speed of 150 rpm for a predetermined time, before filtration to separate the metal ion solution and spent adsorbent. The metal ion concentration was measured before and after the adsorption using direct titration with a standard EDTA solution.

The amount of adsorbed Hg(II) at equilibrium, q_e (mg/g) was calculated using:

$$q_e = \frac{(C_o - C_e).V(l)}{W} \tag{1}$$

While the percentage removal was calculated using:

$$\text{Removal\%} = \frac{C_o - C_e}{C_o} \cdot 100\% \tag{2}$$

where C_o and C_e (mg L^{-1}) are the initial metal concentration and metal concentration at equilibrium, W (g) is the weight of the adsorbent and V (L) is the volume of Hg(II) solution analysed.

2.2.3. Carboxylic group content

Adsorbent samples were analysed for carboxylic group contents [18] by adding 0.2 g of the adsorbent to a 125 mL flask containing 50 mL NaOH solution (0.03 N). The flasks were left overnight at room temperature, after which the contents were titrated with standard HCl solution (0.01 N) using a phenolphthalein indicator. The carboxylic group content of the adsorbent sample was calculated using:

$$[COOH]m.eq/100g\ sample = \frac{(V_0 - V_l) \cdot N \cdot 100}{wt} \tag{3}$$

where V_o is the HCl volume (mL) consumed without the addition of the adsorbent within the blank experiment, V_l is the HCl volume (mL) consumed by the adsorbent sample, N is the normality of the HCl solution and W is the weight of the adsorbent sample (g).

2.2.4. Characterization of the adsorbent

MCC, TMCC, and post-adsorption TMCC loaded with Hg(II) were characterised using Fourier Transform infrared spectroscopy (FTIR) to assign vibrational frequencies of the functional groups present within the structures; this technique also provides insight into the character of any bonds formed between Hg(II) ions and the adsorbent surface. FTIR spectra of KBr discs containing ∼2-10 mg of sample in ~∼300 mg of KBr were recorded employing a Perkin–Elmer Spectrum 1000 spectrophotometer over a wavelength range of 4000–400 cm^{-1}, at a scan-interval of 1 cm^{-1} over 120 scans.

A sample of each adsorbent was coated with chromium on carbon tape then imaged employing a TESCAN CE VEGA 3 SBU (117-0195- Czech Republic) scanning microscope (SEM). Images were recorded using 1000 x magnification.Energy-dispersive X-ray (EDX) patterns were recorded using a dispersive X-ray fluorescence (EDX) spectrometer (Oxford Instruments) attached to a scanning microscope (JEOL-JSM-5600). The test was performed on post-adsorption TMCC samples to establish the presence or absence of Hg(II) ions using the characteristic band of mercury metal for confirmation.

The textural characteristics of TMCC were determined via nitrogen adsorption using an Autosorb I assembly. The analysis was conducted using oxygen-free nitrogen gas (Nova 2000, Quanta Chrome Instrument, Beach, USA) at-196 °C, and the isothermal data obtained was analysed using the Brunauer-Emmett-Teller method. Mesopore volume, external area, and mesopore area were calculated using the t-plot method, while the Barrett-Joyner-Halenda technique was utilised to determine the average pore width and pore size distribution.

A solid addition method was used to evaluate the pH at the point of zero charge (pH_{pzc}) for TMCC. 100 mL of 0.01 N NaCl was added to a series of conical flasks, and the pH adjusted within the range 2 to 12, using an aqueous solution of 0.01 N HCl and 0.01 N NaOH. The initial pH was recorded after a constant pH value was attained; thereafter, 100 mg of the adsorbent was dispersed in the conical flasks and incubated for 24 h to obtain the final pH. The initial and final pH values were plotted, with the point of intersection of the plots denoting the pH_{pzc} of the adsorbent.

3. Results and Discussion

3.1. Adsorbent characterization

Modification of MCC by BTCA was confirmed by comparison of the surface functional characteristics of MCC, TMCC, and TMCC loaded with Hg(II) ions. The spectra of virgin MCC (Figure 1a), demonstrated bands at 3326 cm^{-1} (stretching frequency of -OH group), 2892 cm^{-1} (C-H stretching vibration), 1644 cm^{-1} (bound water absorption [26,27]), 1429 cm^{-1} (-CH_2 scissoring) indicative of the carbohydrate character. The absorption peak at ~1023 cm^{-1} (C-O stretching vibration) indicates the presence of the glucose ring, the intensity of which was unchanged by modification, as expected. New peaks are observed for TMCC, Figure 1b; 1715 cm^{-1} is assigned to the stretching vibration of the newly formed ester carbonyl groups while the peak at 1428 cm^{-1} is the -OH bending vibration from -COOH. These peaks indicate the successful modification of MCC with BTCA. The spectrum obtained for TMCC loaded with Hg(II) ions show a shift in peaks observed at observed at 1715, 1645, 1317, 662, 592 and 555 cm^{-1} to 1714, 1644, 1316, 6621, 588 and 554 cm^{-1}, and new peaks at 1202, 1026, 890 and 439 cm^{-1}, which are attributable to the qualitative observation of the adsorption of Hg(II) ions onto the adsorbent.

Figure 2a show the surface morphology of TMCC, which is an agglomerated material with a evident porous character; no obvious changes were observed upon adsorption of Hg(II) ions (Figure 2b), which supports the application of this adsorbent in a commercial system for water remediation. The EDX spectra of Hg(II)-loaded TMCC is presented within the chart of Figure 2c. The presence of sharp peaks, which correspond to elemental Hg, within the EDX spectra (Figure 2c) confirms the adsorption of Hg(II) onto the TMCC surface.

Textural analysis of MCC shows that it has a BET surface area of 2.9 $m^2\ g^{-1}$, and a total pore volume of 0.004 $cm^3\ g^{-1}$. The average pore width is, within the mesoporous region [28] at, 5 nm which is beneficial for mass transport, particularly in aqueous systems. The textural properties are unaffected by treatment with BTCA to form TMCC.

3.3. Factors affecting adsorption of Hg(II) onto TMCC

Point of Zero Charge(pH_{pzc}) The effect of pH on the adsorption of Hg(II) ions by TMCC (pH 2.0–5.0) for an initial Hg(II) ion concentration of 300 mg/L is shown in Figure 3.The adsorption of Hg(II) ions increased from 16 to 308 mg/g by increasing the pH from 2.0 to 5.0; at low (more acidic) pH the high concentration of protons in solution shifts the equilibrium in Equation 4, shown below and representing deprotonation, to the left, hence, the -COOH groups are not ionised and ion exchange sites on the TMCC surface remain protonated and Hg(II) ions are not adsorbed (i.e. Equation 5 cannot occur as efficiently). Under these solution conditions, the bulk of the metal ion is in solution. As the pH increases from 3 to 5, the adsorption capacity of Hg(II) increases due to the decrease in protons in solution.

$$2MMCC - COOH \Leftrightarrow 2MMCC - COO^{-} + 2H^{+} \tag{4}$$

$$2MMCC - COO^{-} + Hg^{2+} \Leftrightarrow (MMCC - COO)_2 \cdot Hg \tag{5}$$

The pH_{pzc} determines the pH at which the surface of TMCC has neutral charge, for this system this occurs at pH 4.0, and maximum adsorption happens at pH values higher than this, where the surface is predominately negatively charged [29]. The pH_{pzc} can also be used to infer the electrostatic interaction between the surface of adsorbent and adsorbate [30]; in this case, pH values lower than the pH_{pzc}, would cause the surface charge of the adsorbent to become positively charged, thereby, making the adsorption of cations is unfavourable [31], hence, the lower amounts adsorbed, while, pH values above the pH_{pzc}, result in the charge of the TMCC surface being negative and favouring the binding of cations, so pH 5.0 (Figure 3) leads to electrostatic attraction between the Hg(II) ions and negatively charged surface [32] enhancing adsorption.

Effect of adsorbent concentration Adsorbent doses within the range of 0.3–10 g/L, at an initial metal ion concentration of 300 mg/L and pH 5.0, were used to probe the effect of adsorbent quantity on adsorption capacity of TMCC (Figure 4). The adsorption capacity (q_e) of Hg(II) ions per unit mass of adsorbent decreased from 308 to 33 mg/g with increasing adsorbent dose, a plateau was observed at the highest dosing levels. The observed decrease in adsorption capacity can be ascribed to a high degree of unsaturated adsorption sites on the increased number of adsorbent particles, which can also become crowded in the system [33].

Effect of contact time The adsorption capacity of TMCC towards Hg(II) ions at three different initial adsorbate concentration of 274, 328 and 600 mg/l is shown as a function of contact time in Figure 5. The capacity increased with increasing contact time and initial adsorptive concentration, before establishing a plateau at times greater than 120 min.

3.4 Isotherm Modelling

The adsorption equilibrium of Hg(II) ions by TMCC was studied using a range of isotherm models. The Langmuir equation [34], is based on homogeneous, monolayer adsorption onto energetically equivalent, localised sites without any surface migration, and the non-linear form of the model is represented by:

$$q_e = \frac{k_L.C_e}{1 + a_L.C_e} \quad (6)$$

where K_L refers to the Langmuir constant (L/g), a_L is the Langmuir isotherm constant (L/mg), and k_L/a_L is the maximum adsorption capacity (Q_{max}).

The Freundlich isotherm is often applied to multilayer adsorption on a heterogeneous surface, where the energies of the localised sites falls off logarithmically. The logarithmic form of this model is expressed by [35]:

$$q_e = K_F.C_e^{1/n} \quad (7)$$

Where C_e is the concentration of Hg(II) ions at equilibrium (mg/L), qe is the amount of adsorbed Hg(II) ions per unit of weight (mg/g), and K_F and n are Freundlich constants associated with the adsorption capacity and favourability, respectively.

The Temkin isotherm model [36], by contrast, assumes that the decrease of surface site energies is linear. The non-linear Temkin isotherm model is given by:

$$q_e = \frac{RT}{b_T} \ln(A_T C_e) \tag{8}$$

where A_T is the Temkin isotherm constant (l/g), b_T is the Temkin constant of adsorption (J/mol), T is absolute temperature (K), and R is the universal gas constant.

The Dubinin-Radushkevich isotherm model [37] is generally expressed as follows:

$$q_e = q_D.\exp(-B_D[RT\ln(1+\frac{1}{C_e})]^2) \tag{9}$$

where q_D and β_D are Dubinin-Radushkevich constants and all other terms are as defined above.

The Redlich–Peterson isotherm [38] combines features from both the Freundlich and Langmuir models; the non-linear Redlich–Peterson equation can be represented by:

$$q_e = \frac{A \cdot C_e}{1 + B \cdot C_e^g} \tag{10}$$

Where k_R (L/g) and α_R are the constants of adsorption, and g is an exponent value (0 to 1).

Heterogeneous adsorption systems can also be described by the Toth isotherm [39]; which satisfies both low and high end concentration boundaries, and can be expressed by:

$$q_e = \frac{k_T \cdot C_e}{(a_T + C_e)^{\frac{1}{t}}} \tag{11}$$

Where K_t is the Toth isotherm constant, a_t is the maximum adsorption capacity, and 1/t is the Toth exponent constant. This isotherm reduces to the Langmuir isotherm if t is close to the unity.

The Sips isotherm [40] is another combined form of the Langmuir and Freundlich models, and can be represented by:

$$q_e = \frac{k_s \cdot C_e^{\beta_1}}{1 + a_s \cdot C_e^{\beta_1}} \tag{12}$$

where k_s (l/g) and a_s (L/mg) are the Sips isotherm constants, and β_S is the Sips model exponent. The Sips isotherm reduces to the Freundlich isotherm at low adsorbate concentrations and predicts monolayer adsorption, characteristic of the Langmuir isotherm. at high adsorbate concentrations.

Finally, the Hill model [41] assumes that the adsorption process is a cooperative phenomenon, for example the ligand binding ability at one site on a macromolecule may influence different binding sites on the same macromolecule. It is described by the following equation:

$$q_e = \frac{q_{s_H}.C_e^{n_H}}{k_D + C_e^{n_H}} \qquad 13$$

where k_D, n_H and s_H are constants for the Hill model.

Minimization of the error distribution between the experimental data and isotherm analysis was performed by using error functions for all models used. The error functions used were Average Relative Error (ARE), Average Percentage Error (APE %), Sum Squares Error (ERRSQ/SSE), and Coefficient of determination (R^2) [19-25], as defined in Table 2, and these were optimised by non-linear regression to attenuate the function errors between the experimental data and therefore the data derived from isotherms studied. Figures 6 and 7 show comparisons between experimental and theoretical data for all models studied and fit data is presented in Tables 3 and 4. From the results obtained, it is evident that the Langmuir model provides the most appropriate fit to the experimental data, with the models ordered as Langmuir > Sips > Hill > Temkin >.Toth >.Freundlich > Redlich-Peterson > Dubinin.

3.5 Adsorption kinetics

The equilibrium capacity of an adsorption system must be matched by suitable kinetic performance for potential application of such adsorbents. In the present study four models were used to analyze the kinetics of adsorption for Hg(II) ions on MMCC, namely pseudo-first-order, pseudo-second-order, Bangham, Elovich and intra-particle diffusion models. As for the adsorption models discussed above, the same series of fitting functions were used to determine the quality of the fits between experimental theoretical data.

The pseudo-first order model is based on a physical and diffusion controlled process; the non-linear form of the model [42] is given by:

$$q_t = q_e[1 - \exp(-k_1 t)] \tag{10}$$

where q_t is the amount of Hg(II) ions adsorbed ($mg.g^{-1}$) at time t (min), q_e is the amount of Hg(II) ions adsorbed ($mg.g^{-1}$) at equilibrium and k_1 is the rate constant (min^{-1}).

The pseudo-second order kinetic model [43] is assumed to involve physicochemical interactions between the adsorbent and adsorbate; the non-linear form of the model given by:

$$q_t = k_2.q_e^2.t/(1 + k_2.q_e.t) \tag{11}$$

Where q_t, q_e and t are as defined above, and k_2 ($g.mg^{-1}$ min^{-1}) is the rate constant for the kinetic model.

Diffusion mechanisms cannot be elucidated by either the pseudo-first-order or pseudo-second-order kinetic models, hence, the intra-particle diffusion model is also used to evaluate the kinetic results. The overall kinetics of adsorption when controlled by intra-particle diffusion [44] can be expressed by:

$$q_t = k_{id}.t^{0.5} + C \tag{12}$$

where q_t and t are as defined above, k_{id} ($mg.g^{-1}min^{1/2}$) is the intra-particle diffusion rate constant, C ($mg.g^{-1}$) is the concentration of Hg(II) at equilibrium. Previous studies reported that that the plots of q_t vs. $t^{1/2}$ are multi-linear steps controlled the adsorption process [45, 46]. Initially a curve is observed, indicative of bulk diffusion, followed by a linear portion, attributed to intra-particle diffusion, and finally a plateau once equilibrium is achieved.

Bangham's kinetic model can be used to determine whether pore diffusion is the only rate-controlling step [47], through the quality of the fit, and is expressed by Equation 13:

$$q_t = q_e[1 - \exp(-k_b.t^n] \qquad (13)$$

where q_t, q_e and t are as defined above, and k_b is the rate constant for the model.

The Elovich model equation [48] is generally expressed as:

$$q_t = \beta.\ln(\alpha.\beta.t) \qquad 18$$

where α (mg. g^{-1}. min^{-1}) is the initial adsorption rate and the parameter β (g. mg^{-1}. L) is related to the extent of surface coverage and activation energy for chemisorption.

Error analysis was conducted in line with the methods used to determine appropriateness of the isotherm models, as well as hybrid fractional error function (HYBRID), Marquardt's percent standard deviation MPSD, sum of absolute error (EABS), and nonlinear chi-square test (χ^2), as defined in Table 2. Fits to the five kinetic models are shown in Figures 10-13; overall, the results obtained from the four kinetic models and data of all error functions used show that the adsorption kinetic models could be ordered: pseudo-first-order > Bangham > pseudo-second-order > Elovich > intra-particle for quality of fit to the experimental data obtained for the adsorption of Hg(II) ions onto TMCC, which indicates that the process is a physical one.

3.6 Adsorption Thermodynamics

The effect of temperature is crucial in determining the working capacity of any prospective adsorbent under the conditions of use. Here, the adsorption capacity of Hg(II) ions onto TMCC was studied at pH 5.0 and an adsorbent dose of 0.3 g L^{-1}, at 30, 50, and 60°C (Figure 13). Thermodynamic parameters, including the standard free energy (ΔG°), enthalpy change (ΔH°) and entropy change (ΔS°) were calculated through the application of Equations 14-16 [52]. The standard free energy (ΔG°) was calculated from the relationship:

$$\Delta G^{\circ} = -RT \ln a_L \tag{14}$$

where a_L is the Langmuir constant, R is the universal gas constant (8.31441 J/mol·K) and T is the absolute temperature (K). The Langmuir constant, a_L, can be used in the van't Hoff equation to determine the enthalpy change, ΔH°, of the adsorption process as a function of temperature as follows:

$$\ln\left(\frac{a_{L2}}{a_{L1}}\right) = \frac{\Delta H^o}{R} \cdot \frac{(T_2 - T_1)}{T_1 . T_2} \tag{15}$$

where a_{L1}, a_{L2} and a_{L3} are the Langmuir constants at 30, 50 and 60 °C, respectively. The positive values of ΔG° obtained using Equation 14 and listed in Table 6 indicate the spontaneous nature of the adsorption of Pb(II) ions onto MMCC, which may be related to the chemical interactions of complexation. Additionally, a negative value was obtained for ΔH° in the range of 30–60 °C, using Equation 15 and is shown in Table 6; which suggests that the adsorption process of Pb(II) ions onto MMCC is exothermic over this temperature range, indicative of a physisorption process. Finally, the entropy change (ΔS°) was calculated from Equation 16:

$$\Delta G^o = \Delta H^o - T\Delta S^o \tag{16}$$

and the negative value of ΔS° in the range of 30–60 °C, is related to an decrease in randomness at the solid/solution interface during the adsorption of Pb(II) ions onto MMCC, as expected for adsorption of solute from an aqueous media.

3.7 Mechanism of adsorption

The data obtained in this study indicate that the TMCC adsorbent is rich in carboxylic functionalities on its surface, which, at the pH used here, has a negative charge that attracts the positively charged Hg(II) ions from aqueous solution. It is possible that this occurs in conjunction with complexation between the electron-accepting Hg(II) ions and the electron-donating oxygens on the carboxylic moieties, as shown in Scheme 2.

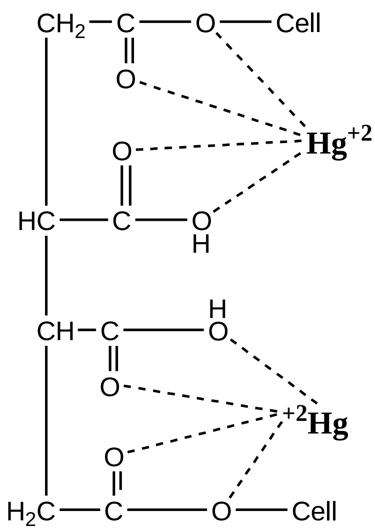

Scheme 2: Complex structure between TMCC and Hg(II) ions.

4. Conclusions

Microcrystalline cellulose were modified by treatment using 1, 2, 3, 4- butanetetracarboxylic acid at elevated temperatures to obtain treated microcrystalline cellulose (TMCC) with a range of carboxylic group contents. The adsorbent samples were characterised for surface group character, which confirmed the incorporation of carboxylic functionalities, surface morphology, shown to remain unchanged during treatment and surface charge, allowing optimisation of adsorption parameters for the target system. The samples were utilised for adsorption of Hg(II) from aqueous solution and the results indicate that the adsorption capacity was optimal at a pH of 5.0 and had a limiting value with adsorbent dose; additionally, at least 120 minutes was required for equilibration of the system and adsorption was seen to increase with increasing temperature. Isothermal modelling showed that the Langmuir model most appropriately described the experimental data, with the model estimating the maximum adsorption capacity according to be 1140 mg/g, at 30°C. The kinetics of adsorption of Hg(II) onto TMCC were analysed using five models, and the pseudo-first-order model showed the best fit for the data obtained in this study, as evaluated using a range of error functions, indicating a physical adsorption process. Thermodynamic analysis indicates that adsorption is non-spontaneous and exothermic, and collectively the data point towards electrostatic interaction between the negatively charged adsorbent and the target cation, which may be stabilised complexation of with the electron-donating deprotonated carboxylic groups. The high capacity of these materials suggest that have potential for use in mercury remediation from the aqueous phase and warrant further study for other heavy metals.

References

[1] Hokkanen, S., A. Bhatnagar, M. Sillanpaa, A review on modification methods to cellulose-based adsorbents to improve adsorption capacity, Water Research 91 (2016) 156-173.

[2] Gusain, D.,V. Srivastava, Y.C. Sharma, Kinetic and thermodynamic studies on the removal of Cu (II) ions from aqueous solutions by adsorption on modified sand, J. Ind. Eng. Chem. 20 (3) (2014) 841–847.

[3] Falayi,T., F. Ntuli, Removal of heavy metals and hromateation of acid mine drainage with un-activated attapulgite, J. Ind. Eng. Chem. 20 (4) (2014) 1285–1292.

[4] Janin, A., J.F. Blais, G. Mercier, P. Drogui, Selective recovery of Cr and Cu in leachate from chromate copper arsenate treated wood using chelating and acidic ion exchange resins, J. Hazard. Mater. 169 (1–3) (2009) 1099–1105.

[5] Bratskaya, S.Y., A.V. Pestov, Y.G. Yatluk, V.A. Avramenko, Heavy metals removal by flocculation/precipitation using N-(2-carboxyethyl) chitosans, Colloids Surf. A Physicochem. Eng. Asp. 339 (1–3) (2009) 140–144.

[6] Tran, T.K., H. J. Leu, K.F. Chiu, C.Y. Lin, Electrochemical treatment of heavy metal containing wastewater with the removal of COD and heavy metal ions, J. Chin. Chem. Soc. 64 (5) (2017) 493–502.

[7] Canet, L., M. Ilpide, P. Seta, Efficient facilitated transport of lead, cadmium, zinc, and silver across a flat-sheet-supported liquid membrane mediated by lasalocid A, Sep. Sci. Technol. 37 (8) (2002) 1851–1860.

[8] Cséfalvay, E., V. Pauer, P. Mizsey, Recovery of copper from process waters by nanofiltration and reverse osmosis, Desalination 240 (1–3) (2009) 132–142.

[9] Bhatnagar, A., M.Sillanpaa, A. Witek-Krowiak, 2015. Agricultural waste peels as versatile biomass for water purification e a review. Chem. Eng. J. 270, 244-271.

[10] Dong, Z., W. Yuan, Y. Lib, R. Hua, L. Zhao, Radiation synthesis of crown ether functionalized microcrystalline cellulose as bifunctional adsorbent: A preliminary investigation on its application for removal of ReO_4- as analogue for TcO4-, Radiation Physics and Chemistry 159 (2019) 147–153.

[11] Wojnarovits, L., C.M. Foldvary, E. Takacs, 2010. Radiation-induced grafting of cellulose for adsorption of hazardous water pollutants: a review. Radiat. Phys. Chem. 79 (8), 848–862.

[12] Barsbay, M., O. Güven, Surface modification of cellulose via conventional and controlled radiationinduced grafting, Radiation Physics and Chemistry 160 (2019) 1–8.

[13] Boparai H.K., M. Joseph, D.M. O'Carroll (2011) Kinetics and thermodynamics of cadmium ion removal by adsorption onto nano zerovalent iron particles. J Hazard Mater 186:458–465.

[14] Qi L., F. Teng, X. Deng, Y. Zhang, X. Zhong (2019) Experimental study on adsorption of Hg(II) with microwave-assisted alkalimodified fly ash. Powder Technol. 351:153–158.

[15] Y. Fu, J. Jiang, Z. Chen, S. Ying, J. Wang, J. Hu (2019) Rapid and selective removal of Hg(II) ions and high catalytic performance of the spent adsorbent based on functionalized mesoporous silica/ poly (m-aminothiophenol) nanocomposite. J Mol Liq 286:110746.

[16] Saman N, H. Kong, S.S. Mohtar, K. Johari, A.F. Mansor, O. Hassan, N. Ali, Mat H (2019) A comparative study on dynamic Hg(II) and MeHg(II) removal by functionalized agrowaste adsorbent: breakthrough analysis and adsorber design. Korean J. Chem. Eng. 36:1069–1081. https ://doi.org/10.1007/s1181 4-019-0285-z

[17] Hashem, A., A. J. Fletcher · M. El-Sakhawy, Latifa A. Mohamed, S. Farag, Aminated Hydroximoyl Camelthorn Residues as a Novel Adsorbent for Extracting Hg(II) From Contaminated Water: Studies of Isotherm, Kinetics, and Mechanism, Journal of Polymers and the Environment, 2020, https://doi.org/10.1007/s10924-020-01789-6.

[18] Khalil, M., A. Hashem, A. Hebeish, Carboxymethylation of Maize Starch Starch/Stärke 42 (1990), pp. 60–63.

[19] Kapoor, A., R.T. Yang, Correlation of equilibrium adsorption data of condensable vapours on porous adsorbents, Gas Sep. Purif. 3 (1989) 187–192.

[20] Rangabhashiyam, S., N. Anu, M. Nandagopal, Relevance of isotherm models in biosorption of pollutants by agricultural byproducts, J. Env. Chem. Eng. 2(1) (2014) 398-414

[21] Kumar, K.V., S. Sivanesan, Pseudo second order kinetics and pseudo isotherms for malachite green onto activated carbon: comparison of linear and nonlinear regression methods, J. Hazard. Mater. B136 (2006) 721–726.

[22] Ng, J.C.Y., W.H. Cheung, G. McKay, Equilibrium studies of the sorption of Cu(II) ions onto chitosan, J. Colloid Interface Sci. 255 (2002) 64–74.

[23] Marquardt, D.W., An algorithm for least-squares estimation of nonlinear parameters, J. Soc. Ind. Appl. Math. 11 (1963) 431–441.

[24] Boulinguiez, B., P. Le Cloirec, D. Wolbert, Revisiting the determination of Langmuir parameters application to tetrahydrothiophene adsorption onto activated carbon, Langmuir 24 (2008) 6420–6424.

[25] Vijayaraghavan, K., T.V.N. Padmesh, K.Palanivelu, M. Velan, Biosorption of nickel(II) ions onto Sargassum wightii: application of two-parameterand three-parameter isotherm models. J. Hazard. Mater. 133 (2006), 304-308.

[26] Ahsan, H. Muhammad, X. Zhang, Y. Li, B. Li, S. Liu, Surface modification of microcrystalline cellulose: Physicochemical characterization and applications in the Stabilization of Pickering emulsions, International Journal of Biological Macromolecules 132 (2019) 1176–1184.

[27] Shi, C., F.Tao, Y. Cui, Evaluation of nitriloacetic acid modified cellulose film on adsorption of methylene blue, International Journal of Biological Macromolecules 114 (2018) 400–407.

[28] Kong, S., X. Huang, , K. Li and X. Song (2019). Adsorption/desorption isotherms of CH_4 and C_2H_6 on typical shale samples. Fuel, 255, 115632.

[29] Hamdaoui, O., Batch study of liquid-phase adsorption of methylene blue using cedar sawdust and crushed brick, J. Hazard. Mater. 135 (2006) 264–273.

[30] Ngah,, W.W. L. Teong, R. Toh, M. Hanafiah, Utilization of chitosan–zeolite composite in the removal of Cu (II) from aqueous solution: adsorption, desorption and fixed bed column studies, Chem. Eng. J. 209 (2012) 46–53.

[31] Martín-Lara, M., F. Hernáinz, M. Calero, G. Blázquez, G. Tenorio, Surface chemistry evaluation of some solid wastes from olive-oil industry used for lead removal from aqueous solutions, Biochem. Eng. J. 44 (2009) 151–159.

[32] Chen,H. Y., Zhao, A. Wang, Removal of Cu (II) from aqueous solution by adsorption onto acid-activated palygorskite, J. Hazard. Mater. 149 (2007) 346–354.

[33] Khalil, A.A., H.H. Sokker, A. Al-Anwar, A. Abd El-Zaher, and A. Hashem, Preparation, characterization and utilization of amidoximated poly(AN/MAA)-grafted alhagi residues for the removal of Zn(II) ions from aqueous solution, Adsorption Science and Technology, 27(2009)363-382.

[34] Langmuir, I. The constitution and fundamental properties of solids and liquids. Part I. solids, J. Am. Chem. Soc. 38 (1916) 2221–2295.

[35] Freundlich, H., Über die adsorption in lösungen Zeitschrift für physikalische, Chemie 57 (1907) 385–470.

[36] Temkin,M., Kinetics of ammonia synthesis on promoted iron catalysts Acta Physiochim., URSS 12 (1940) 327–356.

[37] Dubinin, M.M., Modern state of the theory of volume filling of micropore adsorbents during adsorption of gases and steams on carbon adsorbents, Zhurnal Fizicheskoi Khimii. 39 (1965) 1305–1317.

[38] Redlich, O,. D.L. Peterson, A useful adsorption isotherm, J. Phys. Chem. 63 (1959) 1024–1026.

[39] Toth,J., State equations of the solid gas interface layer, Acta Chem. Acad. Hung. 69 (1971) 311–317.

[40] Sips,R., Combined form of Langmuir and Freundlich equations, J. Chem. Phys. 16 (1948) 490–495.

[41] Foo, K.Y., B.H. Hameed, Insights into the modeling of adsorption isotherm systems, Chem. Eng. J. 156 (2010) 2–10.

[42] Lagergren S.K. (1898) About the theory of so-called adsorption of soluble substances. Sven Vetensk Handingarl 24:1–39.

[43] Ho, Y-S, G. McKay (1999) Pseudo-second order model for sorption processes. Process Biochem. 34:451–465.

[44] Weber W.J., J.C. Morris (1963) Kinetics of adsorption on carbon from solution. J. Sanit. Eng. Div. 89:31–60.

[45] Marrakchi F, M. Ahmed, W. Khanday, M. Asif, B. Hameed (2017), Mesoporous-activated carbon prepared from chitosan flakes via single-step sodium hydroxide activation for the adsorption of methylene blue. Int. J. Biol. Macromol. 98:233–239.

[46] Kołodyńska D, P. Hałas, M. Franus, Z. Hubicki (2017) Zeolite properties improvement by chitosan modification—sorption studies. J. Ind. Eng. Chem. 52:187–196.

[47] Tutem, E., R. Apak, C.F. Unal, Adsorptive removal of chlorophenols from water by bituminous shale, Water Res. 32 (1998) 2315–2324.

[48] Chien,S.H., W.R. Clayton, Application of Elovich equation to the kinetics of phosphate release and sorption in soils, Soil Sci. Soc. Am. J. 44 (1980) 265–268.

[49] Gupta, V.K., Equilibrium uptake, sorption dynamics, process development and column operations for the removal of copper and nickel from aqueous solution and wastewater using activated slag: A low-cost adsorbent, Ind. Eng. Chem. Res. 37 (1998) 192–202.

Tables

Table 1: Samples of TMCC (micocrystalline cellulose (MMC) treated with 1, 2, 3, 4-butanetetracarboxylic acid (BTCA)) used in this study.

BTCA(mmol)	Extent of modification (m.eq-COOH/100 g sample)
0	0
2.14	292.4
4.28	521.8
8.55	667.3

Reaction Conditions: MCC, 12.34 mmol/L; reaction temperature, 140 ^{o}C; reaction time, 1h.

Table 2: List of non-linear error functions used in this study.

Error Function	Equation	References
Average Relative Error (ARE)	$ARE = \sum_{i=1}^{n} \left\| \frac{(q_e)_{\exp.} - (q_e)_{calc.}}{(q_e)_{\exp.}} \right\|$	19
Average Percentage Error (APE)	$APE\% = \frac{\sum_{i=1}^{N} \left\| [((q_e)_{\exp.} - (q_e)_{calc.}) / q_{\exp.}] \right\|}{N} x100$	20
Sum Squares Error (ERRSQ/SSE)	$ERRSQ = \sum_{i=1}^{n} [(q_e)_{calc.} - (q_e)_{\exp.}]^2$	21
Hybrid Fraction Error Function (Hybrid)	$Hybrid = \frac{100}{n-p} \sum_{i=1}^{n} [\frac{((q_e)_{\exp.} - (q_e) calc.)^2}{(q_e)_{\exp.}}]_i$	22
Marquardt's Percent Standard Deviation MPSD	$MPSD = (100 \sqrt{\frac{1}{n-p} \sum_{i=1}^{n} [\frac{((q_e)_{\exp.} - (q_e)_{calc.})}{(q_e)_{\exp.}}]^2}$	23
Nonlinear chi-square test(χ^2)	$\chi^2 = \sum \frac{(q_{e.\exp} - q_{e.theoretical})^2}{q_{e.theoretical}}$	24
Coefficient of determination (R^2)	$R^2 = \frac{\sum_{i=1}^{n} (q_{e,calc} - \overline{q_{e,\exp}})^2}{\sum_{i=1}^{n} (q_{e,calc} - \overline{q_{e,\exp}})^2 + \sum_{i=1}^{n} (q_{e,calc} - q_{e,\exp})^2}$	25

Table 3: Isotherm constants and error analysis of two-parameter models for Hg(II) ions adsorption onto TMCC (micocrystalline cellulose (MMC) treated with 1, 2, 3, 4-butanetetracarboxylic acid (BTCA)) at 30 °C.

Isotherm Model	Parameter	Value	Error Analysis	Value
Langmuir	a_L	0.0061 L/mg	ARE	0.2915
	q_{max}	1139.55 mg/g	APE%	2.915
	k_L	6.93 L/g	ERRSQ	5926.9
			Hybrid	8.262
			MPSD	0.0128
			χ^2	8.048
			R^2	0.9989
Freundlich	n	2.51	ARE	0.7471
	K_F	69.82 mg/g	APE%	7.471
			ERRSQ	20428.4
			Hybrid	56.99
			MPSD	0.2093
			χ^2	47.67
			R^2	0.9959
Temkin	A_T	0.0816 L/g	ARE	0.5491
	b_T	11.23 mg/L	APE%	5.491
			ERRSQ	11021.4
			Hybrid	19.55
			MPSD	0.0483
			χ^2	19.14
			R^2	0.9978
Dubinin			ARE	2.085
			APE%	20.85
			ERRSQ	122753.3
			Hybrid	385.0
			MPSD	1.146
			χ^2	76741.8
			R^2	0.9787

Table 4: Isotherm constants and error analysis of three-parameter models for Hg(II) ions adsorption onto TMCC (micocrystalline cellulose (MMC) treated with 1, 2, 3, 4-butanetetracarboxylic acid (BTCA)) at 30 °C.

Isotherm Model	Parameter	Value	Error Analysis	Value
Hill	q_{SH}	1000	ARE	0.3208
	n_H	1.175200065	APE %	3.208
	k_D	289.8696636	ERRSQ	9872.2
			Hybrid	12.16
			MPSD	0.0159
			χ^2	12.35
			R^2	0.9981
Redlich-Peterson	k_g	-406.245619	ARE	0.7531
	α_g	-6.02710044	APE %	7.531
	g	0.597143208	ERRSQ	20765.9
			Hybrid	57.81
			MPSD	0.2121
			χ^2	48.36
			R^2	0.9958
Sips	k_S	3.418782958	ARE	0.2929
	α_S	0.008625467	APE %	2.929
	β_S	1.216596234	ERRSQ	8661.1
			Hybrid	11.53
			MPSD	0.0158
			χ^2	10.96
			R^2	0.9984
Toth	k_τ	68.80917661	ARE	0.7273
	α_τ	0.575638577	APE %	7.273
	$1/\tau$	0.60031328	ERRSQ	20531.2
			Hybrid	54.16
			MPSD	0.1915
			χ^2	46.81
			R^2	0.9958

Table 5: Kinetic model constants and error analysis for the adsorption of Hg(II) ions TMCC (micocrystalline cellulose (MMC) treated with 1, 2, 3, 4-butanetetracarboxylic acid (BTCA)) at different initial concentrations.

Parameter/Error Analysis	**C_o(mg/L)**		
	274	328	600
Pseudo-First-Order			
q_e	273.7	297.7	637.8
K_1	0.0332	0.0794	0.0351
ARE	0.4196	0.8681	2.101
APE %	3.815	7.892	19.10
ERRSQ	301.5	4417.2	122401.1
Hybrid	4.032	22.10	326.7
MPSD	0.0615	0.1212	0.9155
χ^2	4.518	24.04	664.1
R^2	0.9994	0.9941	0.9567
Pseudo Second Order			
q_e	337.7	321.4	660.9
K_2	0.00010	0.00038	0.00018
ARE	0.6640	0.3120	0.3071
APE %	6.036	2.836	2.792
ERRSQ	1913.7	823.5	3235.2
Hybrid	10.02	3.795	7.651
MPSD	0.0697	0.0182	0.0191
χ^2	9.133	3.811	8.021
R^2	0.9961	0.9989	0.9989
Intra-Particle Diffusion			
k_{id}	0.99998	1.00000	1.00001
C	0.00007	0.00002	0.00002
ARE	10.56	10.69	10.85
APE %	96.04	97.19	98.64
ERRSQ	418143.8	682979.5	2995864.0
Hybrid	1892.9	2596.0	5523.8
MPSD	10.15	10.39	10.70
χ^2	48964.4	97781.0	428750.5
R^2	0.0770	0.0840	0.0815
Bangham Model			
q_e	271.5	312.7	642.5
k_b	0.0320	0.1974	0.2041
n	1.015	0.6062	0.5967
ARE	0.4331	0.2381	0.2150
APE %	3.937	2.165	1.954
ERRSQ	312.1	646.0	2505.1
Hybrid	4.309	3.102	5.926
MPSD	0.0673	0.0151	0.0142
χ^2	4.974	3.301	6.468
R^2	0.9993	0.9991	0.9992
Elovich Model			
α	175.1	326.4	13.35
β	17.90	21.66	53.62
ARE	5.902	1.682	1.360
APE %	53.65	15.29	12.36
ERRSQ	45748.6	17231.9	48519.1
Hybrid	567.9	112.6	155.4
MPSD	8.233	0.7769	0.5235
χ^2	242.73	72.67	105.2
R^2	0.9101	0.97820	0.9851

Table 6: Thermodynamic parameters of Hg(II) ions onto TMCC (micocrystalline cellulose (MMC) treated with 1, 2, 3, 4-butanetetracarboxylic acid (BTCA)) at 30 °C.

Temp. (K)	ΔG^o(kJ.mol^{-1})	ΔH^o(kJ.mol^{-1})	ΔS^o(JK^{-1}.mol$^{-1)}$
30	12.855	-2.735	-51.454
50	13.794		
60	15.148		

Figures

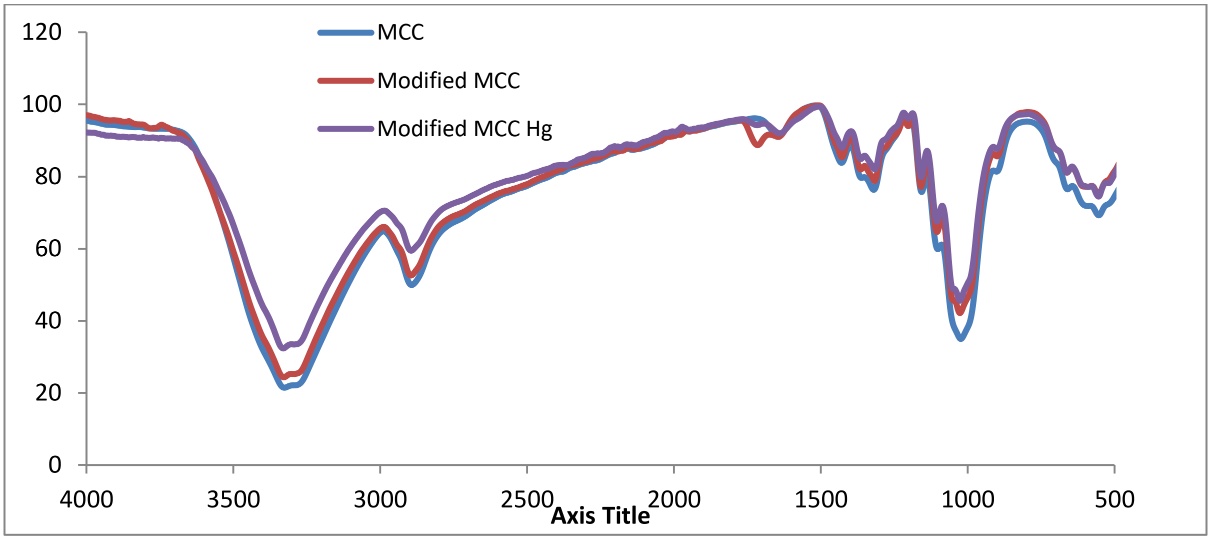

Figure 1: FT-IR spectra of (a) micocrystalline cellulose (MCC); (b) TMCC (micocrystalline cellulose (MMC) modified with 1, 2, 3, 4-butanetetracarboxylic acid (BTCA)); (c) TMCC treated with BTCA and loaded with Hg(II) ions.

(a) **(b)**

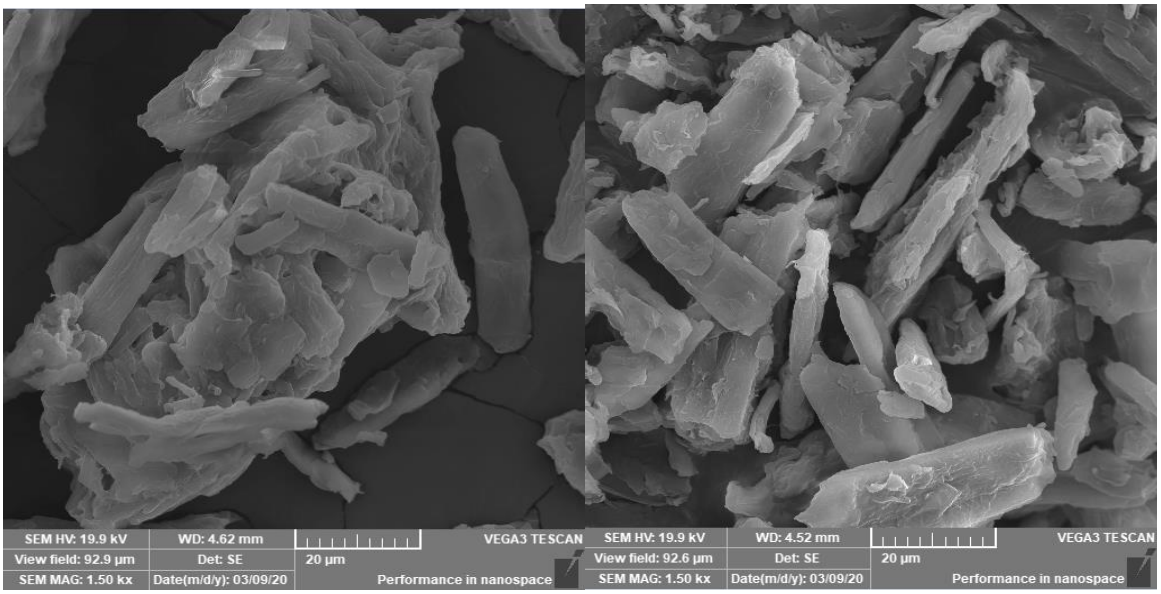

(c)

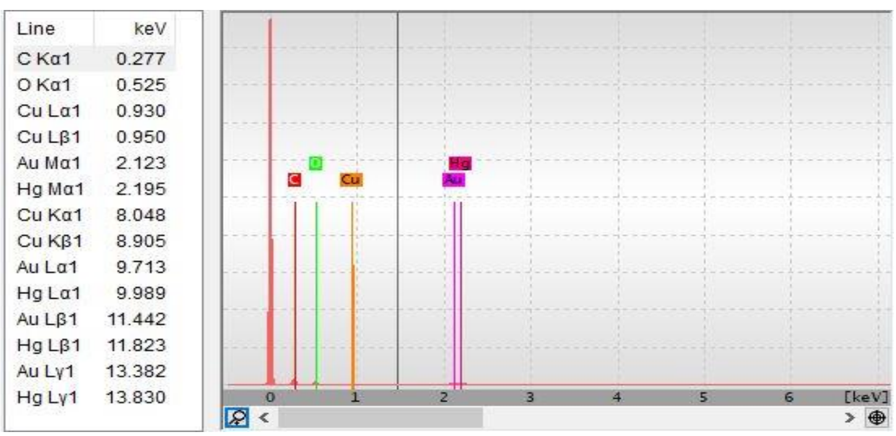

Figure 2: SEM images of (a) TMCC (micocrystalline cellulose (MMC) modified with 1, 2, 3, 4-butanetetracarboxylic acid (BTCA)). (a) TMCC loaded with Pb(II) ions, respectively; (c) associated energy-dispersive X-ray analysis (EDX) patterns for TMCC and TMCC loaded with Hg(II) ions.

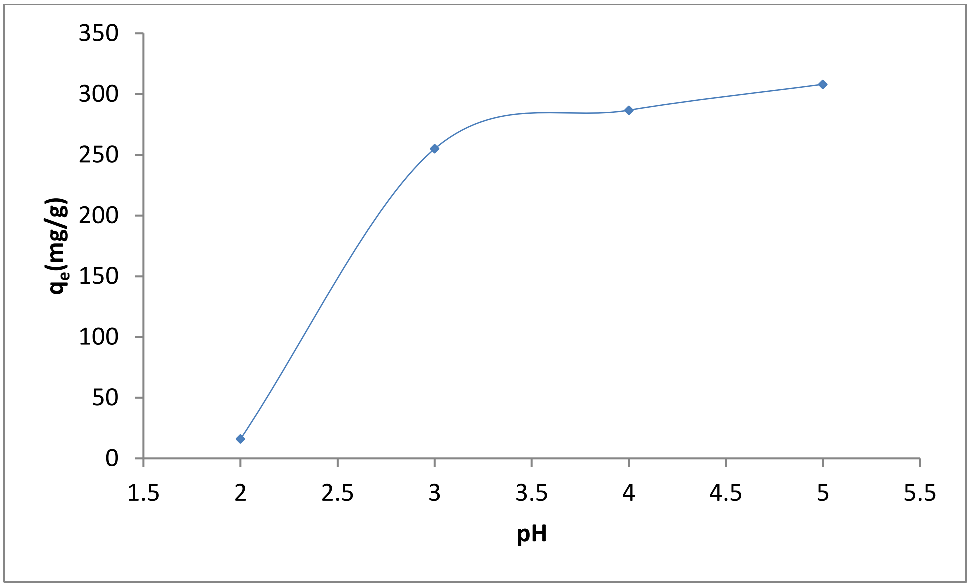

Figure 3: Effect of pH on adsorption capacity of Pb(II) ions onto TMCC (micocrystalline cellulose (MMC) modified with 1, 2, 3, 4-butanetetracarboxylic acid (BTCA)) at 30 °C. Reaction Conditions: Pb(II) conc. 300 mg/L; TMCC conc. 0.3g/L; contact time 2 h; reaction temperature 30 °C; COOH content 231 m.eq/100 g sample.

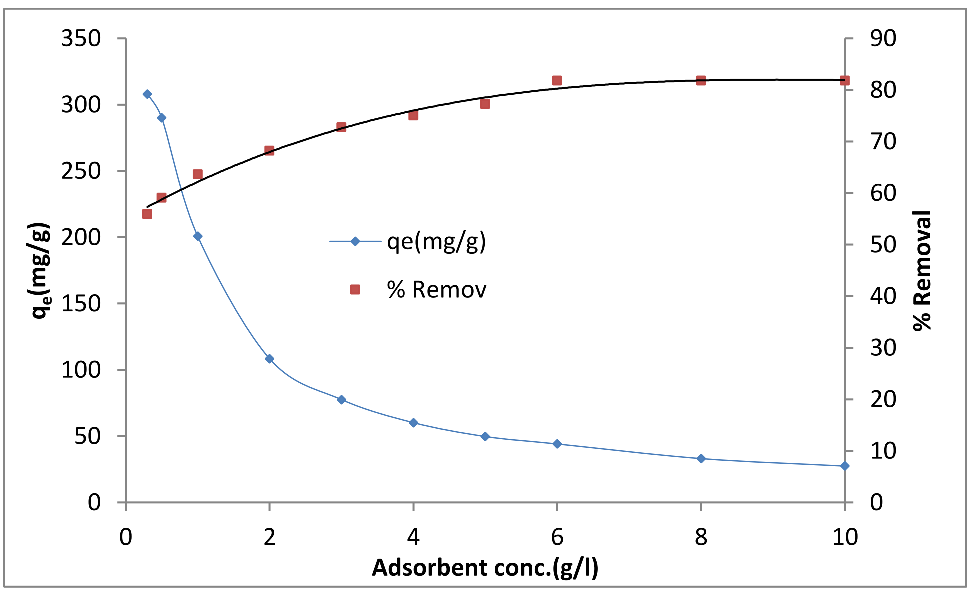

Figure 4: Effect of adsorbent (TMCC) concentration on adsorption capacity of Hg(II) ions onto TMCC (micocrystalline cellulose (MMC) modified with 1, 2, 3, 4-butanetetracarboxylic acid (BTCA)) at 30 °C. Reaction Conditions: Hg(II) conc. 300 mg/L; pH 5; contact time 2 h; reaction temperature 30 °C; COOH content 231 m.eq/100 g sample.

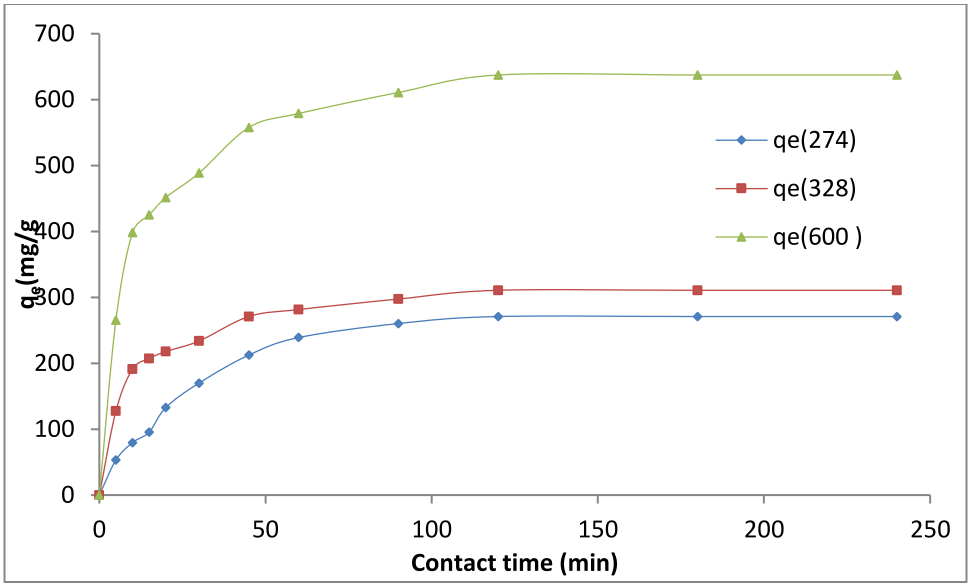

Figure 5: Effect of contact time on adsorption capacity of Pb(II) ions onto TMCC (micocrystalline cellulose (MMC) modified with 1, 2, 3, 4-butanetetracarboxylic acid (BTCA)) at 272, 328 and 600 mg/L. Reaction Conditions: Hg(II) conc. 300 mg/L; pH 5; contact time 2 h; reaction temperature 30 °C; COOH content 231 m.eq/100 g sample.

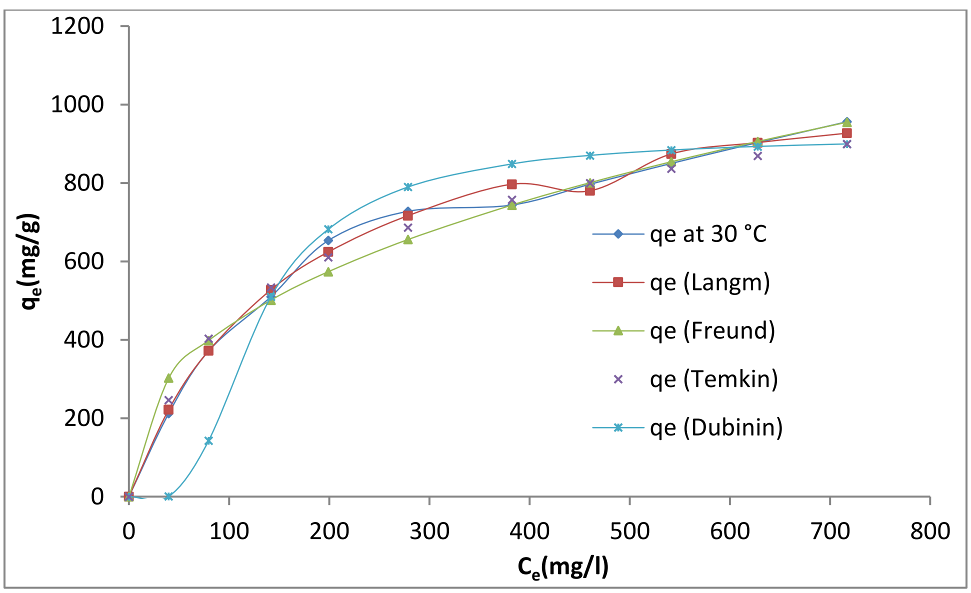

Figure 6: Comparison between experimental data and different two-parameter isotherm models at 30 °C forHg(II) ion adsorption onto TMCC (micocrystalline cellulose (MMC) modified with 1, 2, 3, 4-butanetetracarboxylic acid (BTCA)). Reaction Conditions: TMCC conc. 0.3 g/L; pH 5; contact time 2 h; reaction temperature 30 °C; COOH content 231 m.eq/100 g sample.

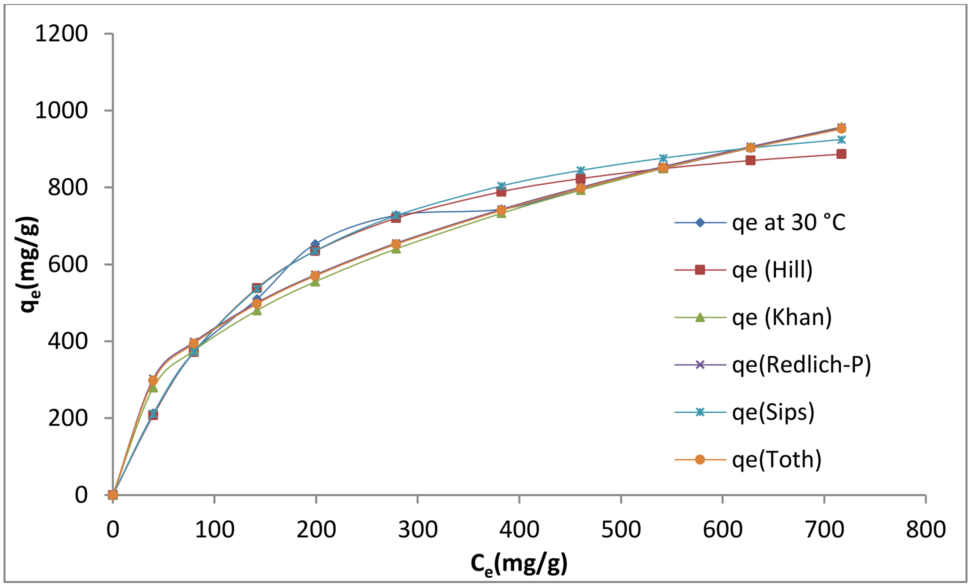

Figure 7: Comparison between experimental data and different three-parameter isotherm models at 30 °C forHg(II) ion adsorption onto TMCC (micocrystalline cellulose (MMC) modified with 1, 2, 3, 4-butanetetracarboxylic acid (BTCA)). Reaction Conditions: TMCC conc. 0.3 g/L; pH 5; contact time 2 h; reaction temperature 30 °C; COOH content 231 m.eq/100 g sample.

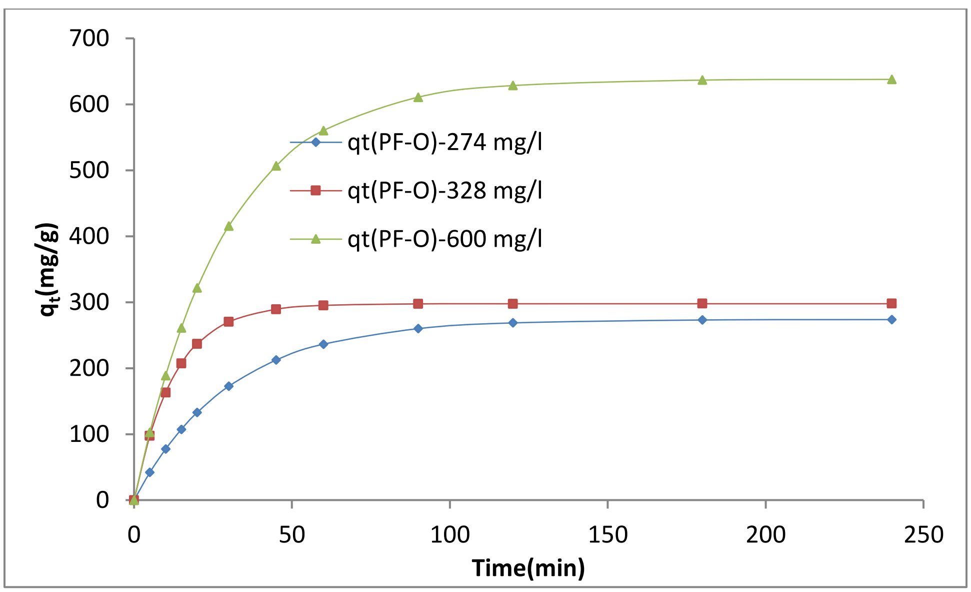

Figure 8: Non-linear plots of pseudo-first order model for adsorption of Hg(II) ions onto TMCC (micocrystalline cellulose (MMC) modified with 1, 2, 3, 4-butanetetracarboxylic acid (BTCA)) at 274, 328 and 600 mg/L. Reaction Conditions: TMCC conc. 0.3 g/L; pH 5; contact time 2 h; reaction temperature 30 °C; COOH content 231 m.eq/100 g sample.

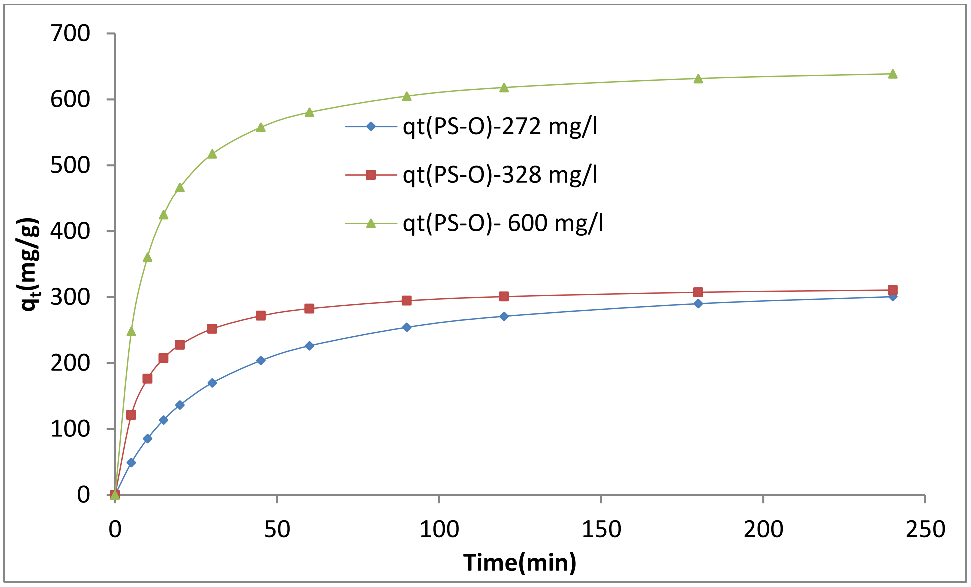

Figure 9: Non-linear plots of pseudo-second order model for adsorption of Hg(II) ions onto TMCC (micocrystalline cellulose (MMC) modified with 1, 2, 3, 4-butanetetracarboxylic acid (BTCA)) at 272, 328 and 600 mg/L. Reaction Conditions: TMCC conc. 0.3 g/L; pH 5; contact time 2 h; reaction temperature 30 °C; COOH content 231 m.eq/100 g sample.

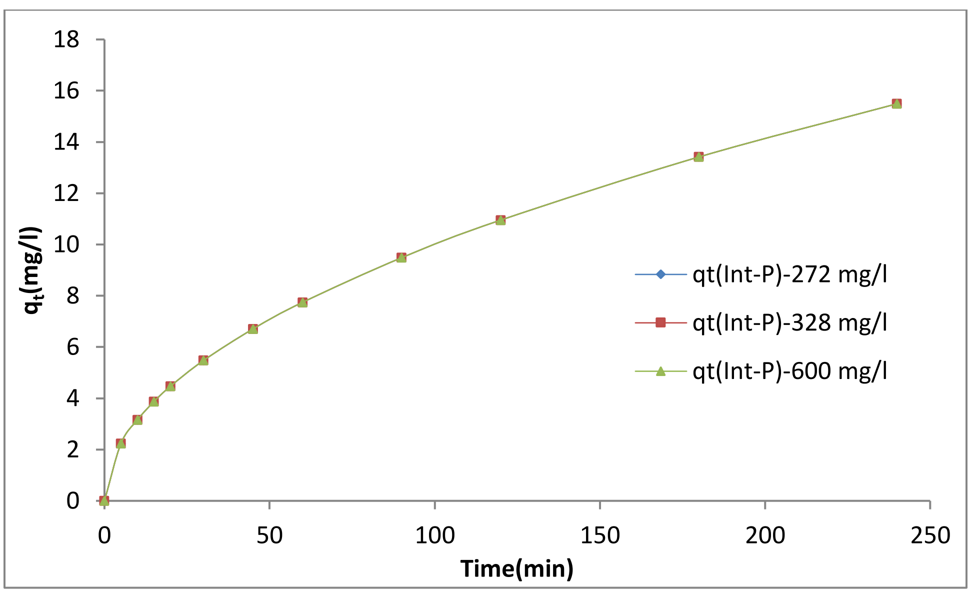

Figure 10: Non-linear plots of intra particle diffusion model for adsorption of Hg(II) ions onto TMCC (micocrystalline cellulose (MMC) modified with 1, 2, 3, 4-butanetetracarboxylic acid (BTCA)) at 303 mg/L and 493 mg/L. Reaction Conditions: TMCC conc. 0.3 g/L; pH 5; contact time 2 h; reaction temperature 30 °C; COOH content 231 m.eq/100 g sample.

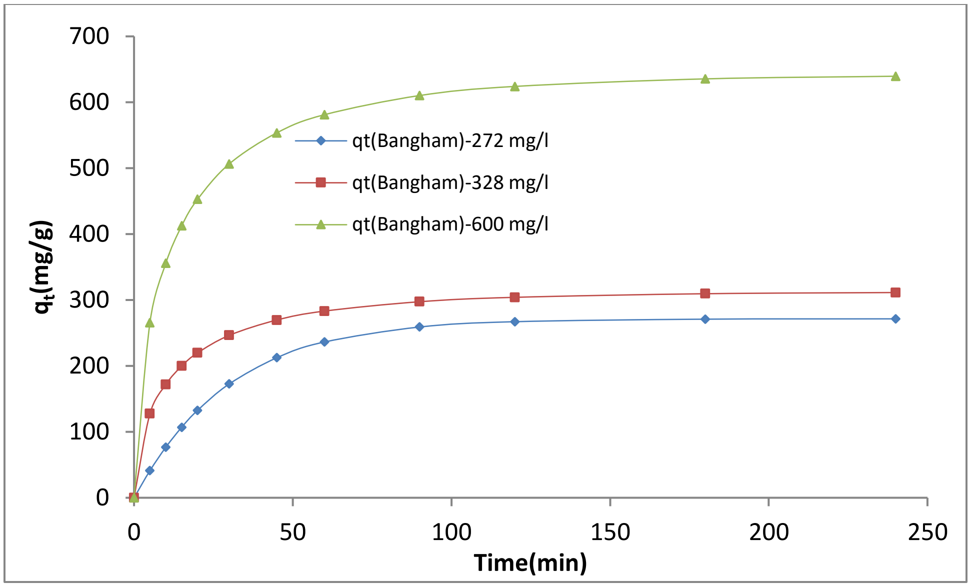

Figure 11: Non-linear plots of Bangham model for adsorption of Hg(II) ions onto TMCC (micocrystalline cellulose (MMC) modified with 1, 2, 3, 4-butanetetracarboxylic acid (BTCA)) at 303 mg/L and 493 mg/L. eaction Conditions: TMCC conc. 0.3 g/L; pH 5; contact time 2 h; reaction temperature 30 °C; COOH content 231 m.eq/100 g sample.

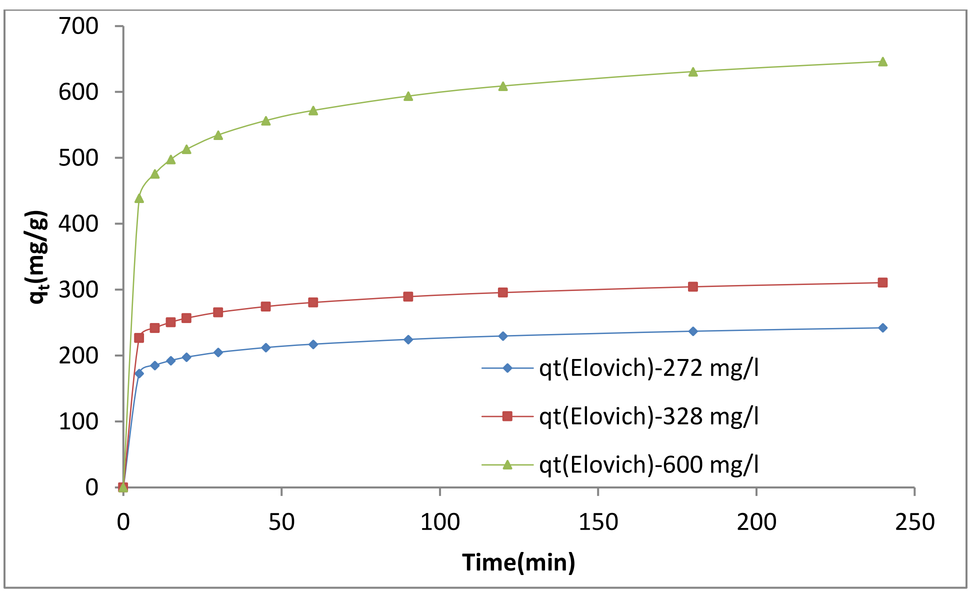

Figure 12: Non-linear plots of Elovich model for adsorption of Hg(II) ions onto TMCC (micocrystalline cellulose (MMC) modified with 1, 2, 3, 4-butanetetracarboxylic acid (BTCA)) at 303 mg/L and 493 mg/L. eaction Conditions: TMCC conc. 0.3 g/L; pH 5; contact time 2 h; reaction temperature 30 °C; COOH content 231 m.eq/100 g sample.

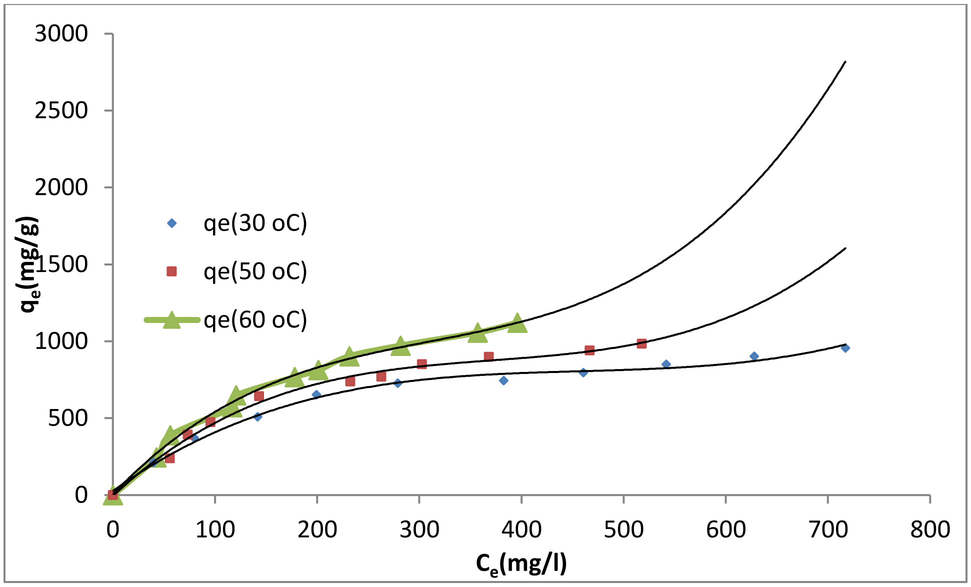

Figure 13: Equilibrium adsorption isotherms of Hg(II) ions onto TMCC (micocrystalline cellulose (MMC) modified with 1, 2, 3, 4-butanetetracarboxylic acid (BTCA)) at 30, 50 and 60 °C. Reaction Conditions: TMCC conc. 0.3 g/L; pH 5; contact time 3 h; COOH content 231 m.eq/100 g sample.